Available online at www.sciencedirect.com

ScienceDirect

Chronic Diseases and Translational Medicine 6 (2020) 198−207

www.keaipublishing.com/en/journals/cdtm/

www.cdatm.org

Original Article

High-fat diet-induced adipose tissue expansion occurs prior to insulin resistance in C57BL/6J mice

Ming-Qian He [a], Jing-Ya Wang [a], Yue Wang [a], Jing Sui [b], Meng Zhang [a], Xi Ding [a], Yang Zhao [a], Zi-Yi Chen [a], Xiao-Xiao Ren [a], Bing-Yin Shi [a,*]

[a] *Department of Endocrinology, The First Affiliated Hospital of Xi'an JiaoTong University, Xi'an, Shaanxi 710061, China*

[b] *Department of Endocrinology and International Medical Center, The First Affiliated Hospital of Xi'an JiaoTong University, Xi'an, Shaanxi 710061, China*

Received 9 November 2019

Available online 18 July 2020

Abstract

Background: To date, there is only scare evidence characterizing the temporal features and progression of metabolic dysfunction in high-fat diet (HFD)-fed obese mice. Hence, its specific pathogenesis remains unclear.

Methods: Sixty 6-week-old male C57BL/6J mice were randomly divided into HFD and control diet (CD) groups and sacrificed at 1, 5, 9, 13, 17, and 21 weeks, respectively. At weekly intervals, intraperitoneal glucose tolerance testing (IPGTT) and intraperitoneal insulin tolerance testing (IPITT) were performed in both groups. A detailed time course in HFD-fed mice was investigated by evaluating the initiation of glucose homeostasis impairment, dyslipidemia, systemic insulin sensitivity, monocyte chemoattractant protein-1 (MCP-1) levels, epididymal white adipose tissue (eWAT) expansion, macrophage content changes, pro-inflammatory (M1)/anti-inflammatory (M2) macrophage imbalance, lipid accumulation in the liver, and β-cell morphometry in the pancreas.

Results: In the HFD group, progressive weight gain and impairments in glucose metabolism (elevated fasting blood glucose and area under the curve (AUC) of IPGTT) were observed from the 3rd week, and a significantly elevated AUC of IPITT was first detected after week 7 of HFD feeding. As for dyslipidemia, after 9 weeks of feeding, the low-density lipoprotein cholesterol level and total cholesterol level in HFD group were significantly higher than those in the CD group (all $P < 0.05$), whereas no significant differences were shown in triglyceride level. Adipocyte size increased significantly in the HFD group in the 1st week, a phenotypic switch in eWAT from anti-inflammatory (M2) to pro-inflammatory (M1) macrophages was observed in the 5th week, and the metabolic inflammation was distinct in eWAT in the 9th week. Additionally, liver steatosis was considerably obvious at the 17th week and pancreatic β-cell morphometry did not change during 21 weeks of HFD feeding.

Conclusion: The eWAT expansion was detected early in HFD-induced obese mice, which occurred prior to obvious insulin resistance.

* Corresponding author. Department of Endocrinology, The First Affiliated Hospital of Xi'an JiaoTong University, 277 West Yanta Road, Xi'an, Shaanxi 710061, China.

E-mail address: shibingy@126.com (B.-Y. Shi).

Peer review under responsibility of Chinese Medical Association.

Production and Hosting by Elsevier on behalf of KeAi

https://doi.org/10.1016/j.cdtm.2020.06.003

Keywords: High-fat diet; Obesity; Metabolic dysfunction; Metabolic inflammation

Introduction

With improvements in standard of living and lifestyle alterations, the morbidity of obesity has increased worldwide, along with several health issues including metabolic syndrome (MS), insulin resistance (IR), type 2 diabetes, and cardiovascular disease.[1,2] Obesity is characterized by a chronic inflammation state initiated by excessive intake of food, especially overconsumption of high-energy processed foods that have abundant sugar and fat.[3] It has been proven that metabolic inflammation may impair insulin signaling in insulin-targeted tissues and disrupt cellular metabolism.[4] However, the temporal features and the progression of metabolic inflammation and dysfunction in high-fat diet (HFD)-induced obesity patients remain unclear.

In the past few years, several animal models have been widely used in studies on the mechanisms and pathophysiology of MS in obesity.[5] One of the most popular models is the genetic animal model, which has been proven to be a good tool to study the pathophysiology and molecular mechanisms of MS as well as its accompanying disorders.[6] Nevertheless, these models are based on either monogenic mutation or beta cell destruction. Even if the genetic animal models have the typical characteristics of MS, they have relatively little clinical relevance. Moreover, it is reported that excessive fat intake may cause insulin insensitivity and obesity,[7] and the role of lipid overload and ectopic fat deposition is highlighted in obesity-related inflammation. Consequently, the HFD-induced obesity mouse model is well-established and commonly used. Such a model is characterized by rapid weight gain as well as metabolic dysfunction, leading to IR.[8,9]

The aim of this study was to assess the progression of metabolic dysfunction, the temporal features, and a detailed time course of HFD-induced obesity in wild-type male C57BL/6J mice.

Methods

Ethical approval

This study was strictly conducted following the recommendations from the National Guide for the Care and Use of Laboratory Animals of China, and all animal experiments were approved by the Xi'an Jiaotong University Laboratory Animal Welfare Ethics Review Committee.

Animal diets and housing conditions

A total of sixty 6-week-old male C57BL/6J mice were purchased from Weitonglihua Inc. (Shanghai, China) and housed in a specific pathogen free (SPF) animal facility with a 12 h light: 12 h dark cycle at room temperature (23 ± 2 °C).

All mice were fed a standard rodent maintenance diet *ad libitum* prior to the study and had free access to clean drinking water during the study. The mice were acclimatized for one week and then were randomly divided into two groups ($n = 30$), namely, control diet (CD, D12450J, Research Diets, Inc., USA; 10% fat, 70% carbohydrate, and 20% protein; 3.85 kcal/g) and high-fat diet (HFD, D12492, Research Diets, Inc., USA; 60% fat, 20% carbohydrate, and 20% protein; 5.24 kcal/g, Table S1). Then, they were sacrificed at the 1st, 5th, 9th, 13th, 17th, and 21st week, respectively. This HFD is commonly used to develop diet-induced obesity models.[10,11]

Blood glucose and insulin measurement

Mice were fasted overnight every other week before fasting blood glucose (FBG) and insulin measurements. Blood glucose was tested through the tail vein using the OneTouch UltraEasy Blood Glucose Monitoring System (Anwen, China). Plasma insulin levels were measured by a mouse enzyme-linked immunosorbent assay (Mouse Insulin ELISA by Raybiotech, Shanghai, China).

Intraperitoneal glucose tolerance testing (IPGTT) and intraperitoneal insulin tolerance testing (IPITT)

At weekly intervals, mice were fasted for 4 h (morning fasting) for IPITT and fasted overnight for IPGTT. Blood glucose levels were measured at 0, 30, 60, and 120 min after glucose (2 g/kg) intraperitoneal injection and at 0, 15, 30, 45, and 60 min after insulin

(0.5 unit/kg) intraperitoneal injection. A 100-μL blood sample was collected from the tail vein, and plasma was separated by centrifugation at 956× *g* for 20 min in EDTA-K2-treated microtubes (Kangjian Medical, China). After centrifugation, plasma was stored at −80 °C for future insulin measurement.

Additionally, the homeostatic model assessment (HOMA) was applied to evaluate IR (HOMA-IR) and β cell function (HOMA-β). The calculation was as follows: HOMA-IR = (fasting glucose × fasting insulin)/22.5; HOMA-β = (20 × fasting insulin)/(fasting glucose − 3.5) %. The area under the curve (AUC) for blood glucose was calculated by the linear trapezoidal method for both IPGTT and IPITT.

Tissue and serum collection

At the 1st, 5th, 9th, 13th, and 17th week and at the end of the 21-week study, mice were fasted overnight, and a whole blood sample was collected by retro-orbital bleeding under chloral hydrate anesthesia. Serum was isolated by centrifugation, and aliquots were stored at −80 °C before analysis. The liver, pancreas, and epididymal white adipose tissue (eWAT) were collected immediately after mice sacrifice, quickly frozen in liquid nitrogen, and stored in −80 °C for later analysis.

Measurements of serum monocyte chemoattractant protein-1 (MCP-1) levels and free fatty acids (FFA) in liver suspension

Briefly, liver tissue (100 mg) was homogenized with 1 ml of phosphate-buffered saline. The liver suspension was isolated by centrifugation, and aliquots were stored at −80 °C before analysis. The quantitative measurements of MCP-1 levels in the serum and FFA in liver suspension were performed using a commercial ELISA kit protocol (MCP-1: ml037840; FFA: ml002083; mlbio, China).

Measurements of lipid levels in the serum and liver suspension

Triglyceride (TG) and total cholesterol (TC) in the serum and liver suspension were measured by the HMMPS methods, and low-density lipoprotein cholesterol (LDL-C) in the serum was measured by a selective protection method. All these measurements were performed by commercial kits according to the manufacturer's recommendations (FUJIFILM Wako Pure Chemical Corporation, Japan) with an automatic biochemical analyzer (Hitachi, LABOSPECT008AS, Japan). The relative deviation of kits was less than 10%.

Histological and immunohistochemical analyses

Immediately after mice sacrifice, a representative sample of each tissue (eWAT, liver, and pancreas) was fixed in 10% neutral buffered formalin solution (Fisher Scientific Co. LLC) for 48–72 h. Samples were then dehydrated in a series of graded ethanol solutions, cleared with xylene, embedded in paraffin, cut into 7 μm sections, and stained with hematoxylin and eosin (H&E). Frozen liver sections were embedded in optimum cutting temperature compound (Tissue-Tek; Laborimpex, Vorst, Belgium) and used for Oil Red O staining for the assessment of hepatic steatosis according to the manufacturer's instructions (American MasterTech, Lodi, CA, USA). Image Pro-Plus software (Media Cybernetics, USA) was used to evaluate the degree of steatosis.

To detect macrophage and crown-like structures (CLSs), eWAT sections were stained with anti-F4/80 antibody (1:1000 dilution, GB11027, Servicebio, China). In order to evaluate adipocyte size indirectly, the number of adipocytes per mm^2 was calculated by manual counting of all adipocytes in an area of 4–5 mm^2 with Image Pro-Plus software (Media Cybernetics, USA). CLSs density was counted along with total adipocyte number and was expressed as number per 1000 adipocytes, as previously described.[12]

Pancreata were routinely processed, and a planimetric method was used to measure β-cell mass (BCM) based on a previous study.[13] To identify β-cells, pancreatic sections were immunostained for insulin (using a guinea pig anti-insulin primary antibody, 1:100 dilution, GB13121, Servicebio, China).

RNA isolation and quantitative real-time polymerase chain reaction (PCR)

Epididymal adipose and pancreas tissues were lysed in TRIzol reagent (Invitrogen, CA, USA), which was used to isolate total RNA from frozen tissues following the manufacturer's protocol. RNA quantity and quality were assessed using the NanoDrop ND-2000 spectrophotometer (NadroDrop Technologies, Wilmington, DE, USA). Single-stranded cDNA was synthesized using PrimeScript™ RT reagent Kit (Takara Bio INC., Shiga, Japan). Quantitative real-time PCR was conducted on a Rotor-Gene Q instrument system (Qiagen, Frederick, MD, USA) by using SYBR Green PCR kits (Takara). The relative mRNA level was quantified by the $2^{-\Delta\Delta CT}$ method. PCR sequences for various genes are presented

in Table S2. β-actin or Ppia was utilized as an internal control.

Western blot analysis

eWAT was homogenized with adipose tissue protein extraction reagent (HR7812; bjbalb, Beijing, China). Equal quantities of protein were loaded and separated on 10% SDS-PAGE gels. After electrophoresis, proteins were transferred to immobilon-P polyvinylidene difluoride membranes and blocked with 5% bovine serum albumin (BSA). Then, the membranes were immunoblotted with different primary antibodies: GLUT4 (diluted 1:200), Akt (diluted 1:200), pAkt (phosphorylated at Ser473) (diluted 1:200), and Glyceraldehyde 3-phosphate dehydrogenas (GADPH, diluted 1:500; Santa Cruz, USA). After the membranes were washed, the immunoblots were incubated with a secondary antibody conjugated with horseradish peroxidase, visualized with an ECL detection system (Syngen, Cambridge, UK), and analyzed using ChemiDoc Quantity One software (Bio-Rad Laboratories, Milan, Italy). GADPH was used as a loading control for Glut4, and pAkt was normalized to Akt.

Statistical analysis

Normally distributed data are presented as means and standard deviations (SD) or as medians with interquartile ranges (HOMA-IR, HOMA-β, density, and integrated optical density (IOD) of red oil-stained liver sections). Differences between HFD and CD groups were analyzed by an independent samples *t*-test or Wilcoxon's rank sum test. Statistical analysis was conducted by SPSS for Windows 22.0 (IBM Corp., USA), and a P value of less than 0.05 was considered significant.

Results

General characteristics of HFD-fed C57BL/6J mice

The mean body weight and FBG of C57BL/6J mice in the HFD group (17.14 ± 1.27 g, 4.70 ± 2.49 mmol/L, $n = 30$) and CD group (16.82 ± 0.76 g, 4.31 ± 0.93 mmol/L, $n = 30$) showed no differences at the beginning. Fasting body weight (FWt) of the HFD group mice was increased to 19% above that of the CD group mice only after 1 week, significantly increased after 3 weeks (25.46 ± 1.98 g *vs.* 23.43 ± 1.79 g, Fig. 1A, $P = 0.027$), and continued to progressively increase to 40% above that of the CD mice by 21 weeks (38.56 ± 7.12 g *vs.* 27.44 ± 1.13 g, Fig. 1A, $P = 0.009$).

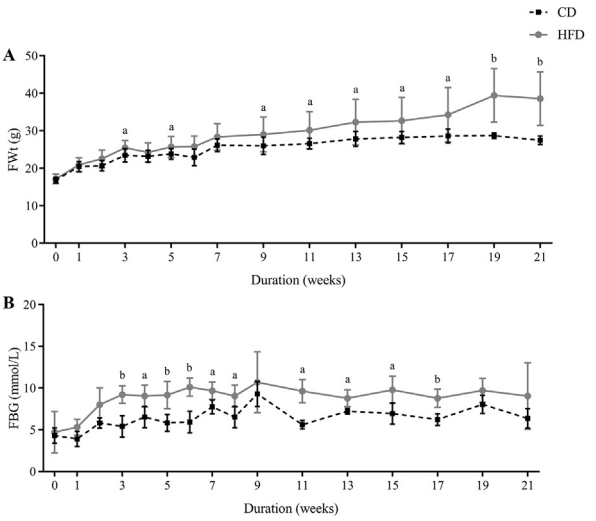

Fig. 1. High-fat diet (HFD) led to progressive hyperglycemia and weight gain. (A) Weekly morning fasting body weight (FWt) measured for 21 weeks in control diet (CD)-fed and HFD-fed mice ($n = 10$/group). (B) Weekly morning fasting blood glucose (FBG) concentrations measured through 21 weeks in CD-fed and HFD-fed mice ($n = 10$/group). All data are presented as means ± SD ($n = 5$). Significance was determined by independent samples *t*-test. $^{a}P < 0.05$; $^{b}P < 0.01$.

Likewise, there was a clear trend for higher FBG levels in HFD-fed mice, and the FBG in the HFD group was significantly higher than that in the CD-fed mice after 3 weeks (9.20 ± 1.05 mmol/L *vs.* 5.42 ± 1.29 mmol/L, Fig. 1B, $P = 0.001$).

Early and progressive impairment of glucose homeostasis in HFD-fed mice

It has been demonstrated that HFD exacerbates the impairments of glucose metabolism in C57BL/6J mice. During IPGTT, HFD induced an increase in FBG and the area under the curve (AUC) after 3-week feeding (Fig. 2A, C). After 7-week HFD feeding, the blood glucose levels were sustained at high levels at each time point, and the blood glucose did not return to normal 120 minutes after intraperitoneal glucose injection (Fig. 2B). Furthermore, the AUC remained significantly elevated during the 21 weeks of HFD feeding (the 21st week: 1832.20 ± 236.08 *vs.* 2349.60 ± 211.14 mmol/L × 120 min, $P = 0.006$).

Meanwhile, IPITT was conducted to evaluate the whole-body insulin sensitivity. During IPITT, after 3-week feeding, a significant increase was only detected in 4-h FBG and 15 min after intraperitoneal insulin injection (Fig. 2C). Notably, after 7-week feeding, the

blood glucose remained elevated in the HFD group 60 min after intraperitoneal insulin injection (Fig. 2E), and the AUC in the HFD group was significantly increased (Fig. 2F), which meant that the insulin-induced hypoglycemic response in HFD-fed mice was impaired. Although no significant increase was found in blood glucose values expressed as percentages of the time 0 value (Fig. 2D, E), the AUC remained significantly elevated during the 21 weeks of HFD feeding (the 21st week: 391.66 ± 50.85 *vs.* 630.18 ± 165.19 mmol/L × 60 min, $P = 0.015$). Therefore, HFD feeding impaired insulin tolerance in mice starting at the 7th week, which was demonstrated by the attenuated action of insulin to lower glucose and the increase in the AUC compared to the CD group (Fig. 2E, F).

Although corresponding insulin secretion profiles in HFD-fed mice tended to be higher (Fig. 2A and B), this was not sufficient to overcome the IR state in these mice. Additionally, the homeostasis model assessment of IR (HOMA-IR) in the 7-week HFD group showed a significantly higher value than that in the CD group (8.45 ± 1.15 *vs.* 5.66 ± 1.51, $P = 0.011$, Table S3), which suggested a state of IR in HFD-fed mice starting from the 7th week. Additionally, the homeostasis model assessment of β (HOMA-β) in the two groups also showed no significant difference ($P > 0.05$, Table S3).

Effects of HFD on lipid levels

A HFD may induce lipid metabolic indisposition, and it always results in hyperlipidemia. To identify dyslipidemia in HFD-fed mice, circulating lipid levels in the serum, including TC, TG, and LDL-C, were measured (Fig. 3). The HFD led to significantly higher LDL-C levels (0.36 ± 0.17 mmol/L *vs.* 0.14 ± 0.02 mmol/L, $P = 0.021$) compared with the CD group after 5 weeks, whereas serum levels of TG and TC showed no significant difference between the two groups. However, after 9-week feeding, LDL-C levels (0.40 ± 0.04 mmol/L *vs.* 0.22 ± 0.14 mmol/L, $P = 0.028$) and TC levels (3.63 ± 0.47 mmol/L *vs.* 2.05 ± 1.03 mmol/L, $P = 0.014$) in the HFD group were significantly higher than those in the CD group, whereas no significant difference was detected in TG levels (0.38 ± 0.07 mmol/L *vs.* 0.42 ± 0.24 mmol/L, $P = 0.676$). Moreover, these lipid level changes remained until the end of the study.

Dynamic changes in epididymal adipose tissue over 21 weeks

To identify the temporal transition point of eWAT dysfunction, mice were fed an HFD for 1, 5, 9, 13, 17, and 21 weeks, and the mean adipocyte size was evaluated at each time point. The H&E staining of eWAT showed an increased adipocyte size in HFD-fed mice starting at the 1st week (Fig. S1). The number of adipocytes per mm^2 significantly decreased after 1 week of HFD feeding, suggesting an increased adipocyte size compared to the CD group (Fig. 4A, $P < 0.01$).

Obesity is commonly related to low-grade inflammation in eWAT, especially the increasing infiltration of adipose tissue macrophages (ATMs). A time-dependent increasing trend was detected in ATM

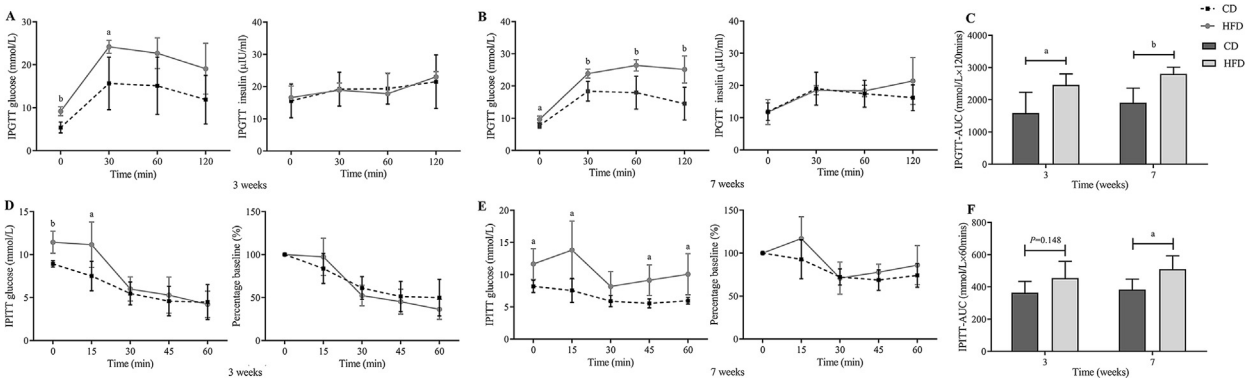

Fig. 2. Progressive glucose intolerance and insulin sensitivity assessed with intraperitoneal glucose tolerance testing (IPGTT) and intraperitoneal insulin tolerance testing (IPITT) in control diet (CD)-fed and High-fat diet (HFD)-fed mice. (A–C) IPGTT (2 g/kg) results (A: blood glucose values, B: the corresponding insulin secretion curves, C: Area under the curve (AUC) for the blood glucose levels) for CD and HFD-fed mice at multiple time points through 3 and 7 weeks of both diets. (D–F) IPITT (0.5 unit/kg) results (D: blood glucose values, E: glucose values expressed as percentages of the time 0 value, F: AUC for the blood glucose levels) for CD and HFD-fed mice at multiple time points through 3 and 7 weeks of both diets. All data are presented as means ± SD ($n = 5$). Significance was determined by independent samples *t*-test. $^{a}P < 0.05$; $^{b}P < 0.01$.

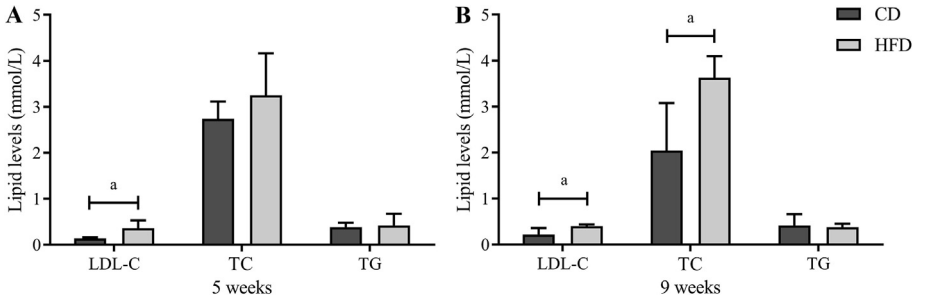

Fig. 3. High-fat diet (HFD) led to progressive hyperlipidemia. The comparative serum lipid levels in two group after 5-week (A) and 9-week (B) feeding. All data are presented as means ± SD ($n = 5$). Significance was determined by independent samples t-test. $^{a}P < 0.05$; $^{b}P < 0.01$. LDL-C: low-density lipoprotein TC: total cholesterol; TG: Triglyceride; CD: control diet.

infiltration in HFD-fed mice. As shown in Fig. S2, eWAT sections were stained with anti-F4/80 antibody to detect ATMs and CLSs (representing an accumulation of macrophages around dead adipocytes) in eWAT. Evidently, CLSs were significantly distinct in HFD-fed mice starting at the 13th week (Fig. 4B and Fig. S2). Likewise, the expression of genes involved in macrophage infiltration, F4/80 in eWAT, was significantly increased from the 13th week in HFD-fed mice compared with those in CD-fed mice (Fig. 4E).

The mRNA expression of pro-inflammatory (M1) and anti-inflammatory (M2) macrophage markers was measured to confirm the presence of eWAT inflammation, and the imbalance between M1/M2 macrophages, which play an important role in the development of IR. In the adipose tissues of mice, the mRNA levels of MCP-1, TNF-α, iNOS, IL6, and IL-1β are used as M1 macrophage markers, and CD206 and Chi3I3 are used as M2 macrophage markers. Our results showed that the mRNA levels of MCP-1, IL6, TNF-α, and iNOS were significantly higher in the HFD groups than in the CD groups from the 9th week of HFD feeding (Fig. 4C, F–H). Moreover, we first spotted obvious elevated MCP-1 concentrations by ELISA (40.638 ± 5.861 *vs.* 49.147 ± 5.047 pg/ml, $P = 0.003$, Fig. 4C) at the 9th week of HFD feeding. In addition, the mRNA levels of CD206 and Chi3I3 were significantly lower in the HFD groups than in the CD groups from the 5th week of HFD feeding (Fig. 4I, J). Taken together, our mouse model suggested a phenotypic switch in adipose tissue from anti-inflammatory (M2) to pro-inflammatory (M1) macrophages starting in the 5th week of HFD feeding, and the metabolic inflammation was distinct in eWAT from the 9th week.

In addition, the protein expression of Glut4 and pAkt (Ser473), and mRNA expression of Glut4 and resistin in eWAT was measured to better understand the insulin signaling and the process of IR in our model. Although the protein expression of pAkt was relatively decreased in the HFD group from the 13th week (Fig. 4M), no significant difference was found in Western blot results. However, the mRNA levels of Glut4 were significantly lower and resistin was significantly higher in the HFD group than in CD group from the 13th week of HFD feeding (Fig. 4K, L), which indicated that IR in eWAT was initially observed at the 13th week of HFD feeding.

Prolonged HFD feeding resulted in lipid accumulation in the liver

In order to evaluate the progression of TG accumulation in the livers of two groups at different times, H&E-stained and red oil-stained liver sections were measured for fatty deposits. H&E-stained sections suggested the occurrence of HFD-induced hepatic steatosis from 17 weeks onwards, which was confirmed by a significant increase in IOD and density in red oil-stained liver sections (Fig. 5 and S3). Additionally, the TG, TC, and FFA concentrations in liver tissue were measured to thoroughly confirm the lipid accumulation in the liver. However, no significant difference was found in liver FFA concentrations. Consistent with the staining result, the TG and TC concentrations in the liver were higher in the HFD groups than in the CD groups from the 17th week of HFD feeding (Fig. 5A), which further confirmed our results.

HFD did not affect pancreatic morphology in C57BL/6J mice

It was observed that HFD did not affect pancreatic morphology during 21-week HFD feeding. Analysis of insulin-containing β-cells in immunohistochemistry sections (Fig. S4) and weight of the pancreas suggested

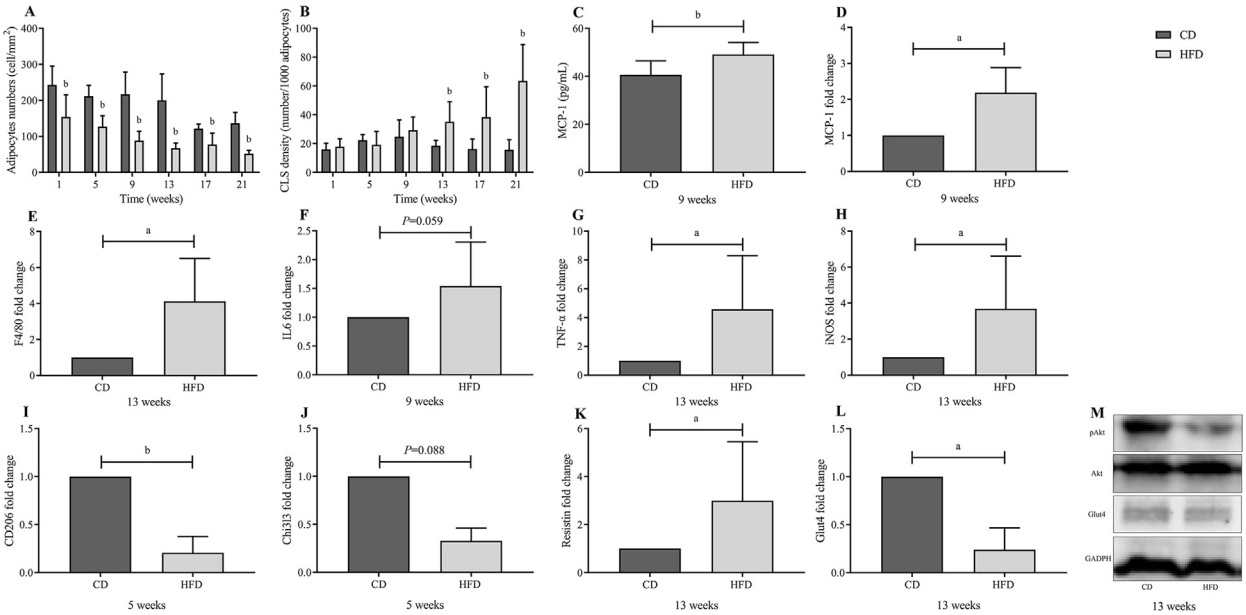

Fig. 4. Dynamic changes in epididymal white adipose tissue (eWAT) over 21-week high-fat diet (HFD) feeding. Histologically quantified number of (A) adipocytes and (B) crown-like structures per mm^2. In the 1st week of HFD, adipocyte size increased significantly. (C) The serum concentrations of MCP-1 in two groups after 9-week feeding. (D−L) mRNA expression levels of macrophage marker (E: F4/80), pro-inflammatory (M1) macrophage markers (D: MCP-1; F: IL6; G: TNF-α; H: iNOS), anti-inflammatory (M2) macrophage markers (I: CD206; J: Chi3l3), and genes responsible for insulin signaling (K: Resistin; L: Glut4). (M) Western blots of insulin signaling molecules (pAkt and Glut4) in eWAT. All mRNA expression data were normalized to control diet (CD) group and are presented as means ± SD ($n = 5$). Significance was determined by independent samples t-test. [a]$P < 0.05$; [b]$P < 0.01$.

that pancreas weights, BCM, islet size, and islet density were not significantly elevated during the 21-week HFD feeding (Fig. S5A−5D). Therefore, no obvious evidence supported the HFD effect on pancreatic morphology in C57BL/6J mice. Additionally, mRNA expression levels of selected β cell functional genes (insulin 1) and selected β cell transcription factors (PDX-1) in pancreatic tissues also revealed that islets were not disturbed by HFD in this study (Fig. S5E and 5F).

Discussion

With the development of the economy and improvements in living standards, the incidence of obesity has reached an alarming rate, and its accompanying metabolic disorders are extremely harmful to human health.[14−16] This urges us to examine the related molecular mechanisms and the detailed progression of this syndrome. Therefore, it is necessary to develop a representative clinically relevant animal model with all the major features of metabolic dysfunction in obesity. In this study, temporal features and the progression of metabolic dysfunction in HFD-fed male C57BL/6J mice were evaluated for 21 weeks.

This study proved that the HFD-fed C57BL/6J mouse is a robust model for metabolic dysfunction in obesity, as described previously.[17−19] FWt, FBG, and AUC of IPGTT were significantly elevated after 3-week HFD feeding, while mice maintained moderate hyperglycemia through 21 weeks with a progressive increase in obesity. Additionally, HFD feeding impaired insulin tolerance in mice from the 7th week, which was demonstrated by the attenuated action of insulin to lower glucose and the increase in the AUC of IPITT compared to the CD group. Similarly, Winzell et al[20] considered HFD-fed mice as an excellent model for studying mechanisms of impaired glucose tolerance. Taken together, the HFD resulted in increased body weight gain and relatively stable hyperglycemia over time.

Adipocytes become hypertrophic through overnutrition; enlarged adipose tissue results in the infiltration of macrophages and imbalance of pro-inflammatory and anti-inflammatory factors secreted by adipose tissue.[21,22] In our mouse model, the HFD induced hypertrophic adipocytes and a phenotypic switch in eWAT from anti-inflammatory (M2) to pro-inflammatory (M1) macrophages, which lead to the promotion of inflammation,

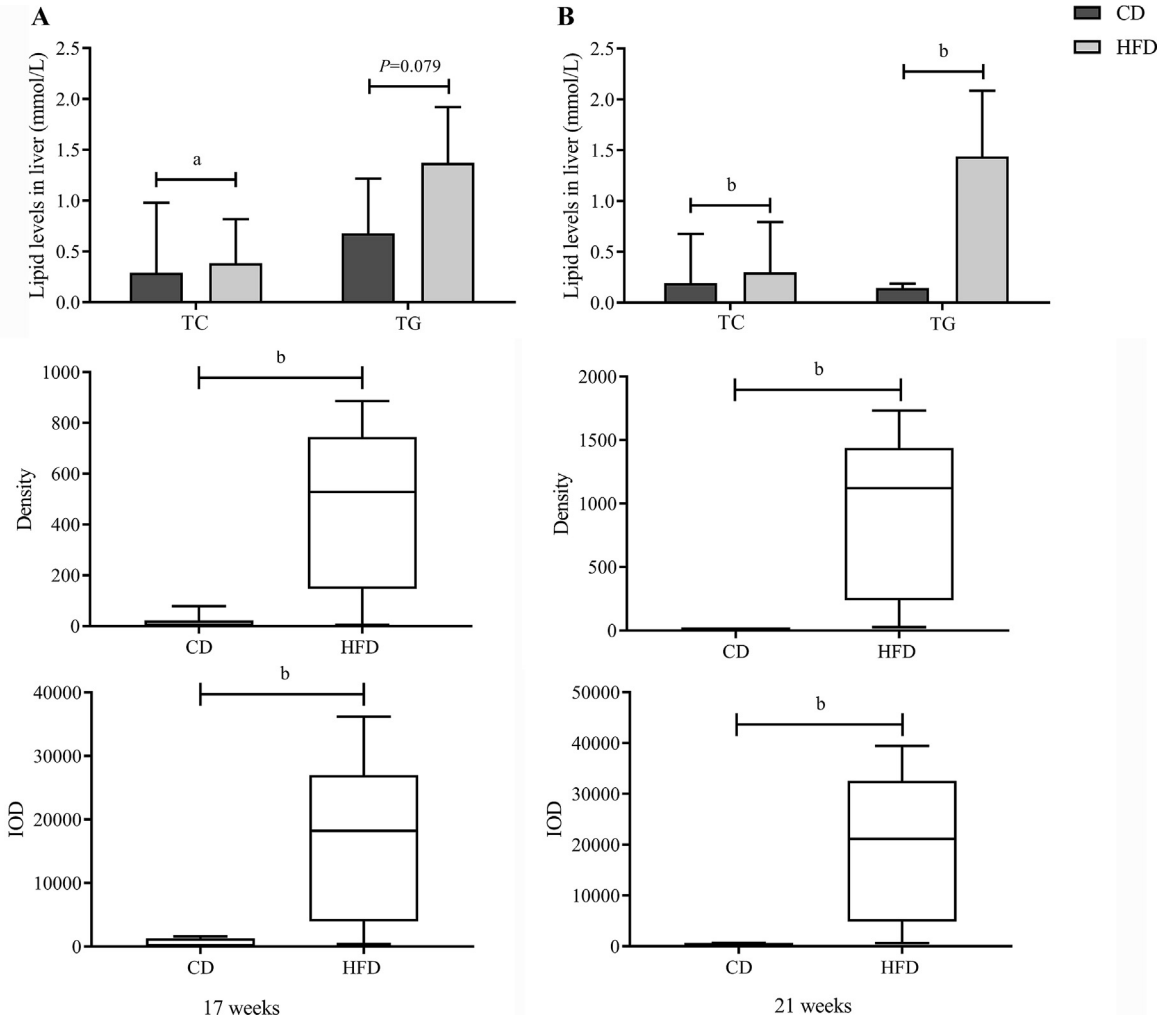

Fig. 5. Prolonged high-fat diet (HFD) feeding resulted in lipid accumulation in the liver. A significant elevation in triglyceride (TG) and cholesterol accumulation in the liver was detected at the 17th week (A) and 21st week (B). Lipid levels are presented as means ± SD ($n = 5$), and significance was determined by independent samples t-test. Density and integrated optical density (IOD) of red oil-stained liver sections are presented as medians with interquartile ranges, and significance was determined by Wilcoxon's rank sum test. $^{a}P < 0.05$; $^{b}P < 0.01$. TC: total cholesterol; CD: control diet.

impairment of insulin sensitivity, and dysregulation of lipid metabolism.[23,24] Accumulating evidence and our study suggested that metabolic low-grade inflammation in eWAT might play an essential role in the development of obesity-related metabolic dysfunction,[10,25,26] resulting in an increase in total serum cholesterol and LDL-C concentrations, and is associated with dyslipidemia.[27] The influence of pro-inflammatory cytokines on lipid metabolism is complex, with the underlying mechanisms still unclear. The pro-inflammatory cytokines play a role in lipid metabolism in different tissues and include a number of metabolic processes, such as inducing lipolysis and increasing FFA production.[26] In addition, pro-inflammatory cytokines regulate cholesterol metabolism and other adipocyte-derived adipokines such as leptin, adiponectin, and resistin, which may also alter lipid metabolism.[26]

In this study, we elucidated the temporal relationship among eWAT inflammation, liver steatosis, and pancreatic β cell expansion in the progression of metabolic dysfunction. Notably, it was revealed that the adipocyte size significantly increased by 1 week of HFD-feeding. Moreover, it was shown that chronic metabolic inflammation was obvious in visceral eWAT depots after 9 weeks of HFD feeding, whilst liver steatosis was obvious from the 17th week, and pancreatic β cell morphological changes did not occur during 21 weeks of HFD feeding. Likewise, Heijden

et al[17] suggested the initial role of eWAT inflammation during the progression of obesity-induced metabolic inflammation. In a word, we provided evidence that obesity-induced eWAT inflammation occurs prior to liver steatosis and pancreatic β cell morphological change, suggesting that eWAT inflammation occurs in the initial phase of metabolic dysfunction in obesity. Consequently, targeting eWAT inflammation might be helpful to ameliorate metabolic dysfunction in obese mice by obstructing its initiation and delaying subsequent progression to other related organs like the liver.[17]

This study identified the temporal features in different tissues responding to HFD, which was related initially to nutritional challenge, primarily in the eWAT expansion and increased inflammation in eWAT, and latterly to liver steatosis. The change of diet composition appeared to take effect in expanding eWAT after 1-week of HFD feeding. The level of sucrose intake in the CD group was identical to that of the HFD group, so that any effect of sucrose on metabolic changes should be identical in the two groups, and any metabolic dysfunction detected should be the result of increased fat content in the diet. This study demonstrated that HFD-induced obesity in mice well-mimicked metabolic dysfunction in human adiposity, providing insight into the prevention and treatment of obesity and the accompanying metabolic disorders.

There are some limitations of this study. Firstly, IPITT was a relatively rough measurement that could not be used identify differences between hepatic and peripheral IR. A future study might utilize hyperinsulinemic-euglycemic clamps to provide more powerful and detailed evidence in this regard. Secondly, due to the time-consuming characteristics of diet experiments and common outliers such as mice without weight gain or mice with abnormal blood glucose levels, the sample size, which should consist of more than 8 mice, was not large enough. Thirdly, the expansion, inflammation, and insulin sensitivity among eWAT, subcutaneous adipose tissue, and brown adipose tissue could not be differentiated.

In conclusion, temporal features underlying the development of metabolic dysfunction during HFD-induced obesity were evaluated in this study. eWAT expansion was detected in the early course of HFD-induced obesity, which occurred prior to obvious IR. Further research is needed for successful extrapolation of the existing evidence to clinical conditions in humans.

Funding

This study was supported by grants from National Key R&D Program of China (No. 2018YFC1311500) and the National Natural Science Foundation of China (NSFC) (No. 81670725 and No. 81970679).

Conflicts of interest

None.

Appendix A. Supplementary data

Supplementary data to this article can be found online at https://doi.org/10.1016/j.cdtm.2020.06.003.

References

1. Hossain P, Kawar B, El Nahas M. Obesity and diabetes in the developing world-a growing challenge. *N Engl J Med*. 2007;356:213–215. https://doi.org/10.1056/NEJMp068177.
2. He M, Shi B. Gut microbiota as a potential target of metabolic syndrome: the role of probiotics and prebiotics. *Cell Biosci*. 2017;7:54. https://doi.org/10.1186/s13578-017-0183-1.
3. Hotamisligil GS. Inflammation, metaflammation and immunometabolic disorders. *Nature*. 2017;542:177–185. https://doi.org/10.1038/nature21363.
4. Samuel VT, Shulman GI. The pathogenesis of insulin resistance: integrating signaling pathways and substrate flux. *J Clin Invest*. 2016;126:12–22. https://doi.org/10.1172/JCI77812.
5. Wong SK, Chin KY, Suhaimi FH, Fairus A, Ima-Nirwana S. Animal models of metabolic syndrome: a review. *Nutr Metab (Lond)*. 2016;13:65. https://doi.org/10.1186/s12986-016-0123-9.
6. King A, Bowe J. Animal models for diabetes: understanding the pathogenesis and finding new treatments. *Biochem Pharmacol*. 2016;99:1–10. https://doi.org/10.1016/j.bcp.2015.08.108.
7. Vessby B, Uusitupa M, Hermansen K, et al. Substituting dietary saturated for monounsaturated fat impairs insulin sensitivity in healthy men and women: the KANWU Study. *Diabetologia*. 2001;44:312–319. https://doi.org/10.1007/s001250051620.
8. Balakumar M, Prabhu D, Sathishkumar C, et al. Improvement in glucose tolerance and insulin sensitivity by probiotic strains of Indian gut origin in high-fat diet-fed C57BL/6J mice. *Eur J Nutr*. 2018;57:279–295. https://doi.org/10.1007/s00394-016-1317-7.
9. Zhang H, Hao Y, Wei C, et al. Chinese medicine Jinlida granules improve high-fat-diet induced metabolic disorders via activation of brown adipose tissue in mice. *Biomed Pharmacother*. 2019;114:108781. https://doi.org/10.1016/j.biopha.2019.108781.
10. Lee YS, Li P, Huh JY, et al. Inflammation is necessary for long-term but not short-term high-fat diet-induced insulin resistance. *Diabetes*. 2011;60:2474–2483. https://doi.org/10.2337/db11-0194.
11. Gupta D, Jetton TL, LaRock K, et al. Temporal characterization of β cell-adaptive and -maladaptive mechanisms during chronic high-fat feeding in C57BL/6NTac mice. *J Biol Chem*.

2017;292:12449−12459. https://doi.org/10.1074/jbc.M117.781047.
12. Murano I, Barbatelli G, Parisani V, et al. Dead adipocytes, detected as crown-like structures, are prevalent in visceral fat depots of genetically obese mice. *J Lipid Res*. 2008;49:1562−1568. https://doi.org/10.1194/jlr.M800019-JLR200.
13. Jetton TL, Lausier J, LaRock K, et al. Mechanisms of compensatory beta-cell growth in insulin-resistant rats: roles of Akt kinase. *Diabetes*. 2005;54:2294−2304. https://doi.org/10.2337/diabetes.54.8.2294.
14. Ford ES. Prevalence of the metabolic syndrome defined by the International Diabetes Federation among adults in the U.S. *Diabetes Care*. 2005;28:2745−2749. https://doi.org/10.2337/diacare.28.11.2745.
15. Toro-MartÃ-n JD, Arsenault BJ, Després JP, Vohl MC. Precision nutrition: a review of personalized nutritional approaches for the prevention and management of metabolic syndrome. *Nutrients*. 2017;9:913. https://doi.org/10.3390/nu9080913.
16. Vassallo P, Driver SL, Stone NJ. Metabolic syndrome: an evolving clinical construct. *Prog Cardiovasc Dis*. 2016;59:172−177. https://doi.org/10.1016/j.pcad.2016.07.012.
17. van der Heijden RA, Sheedfar F, Morrison MC, et al. High-fat diet induced obesity primes inflammation in adipose tissue prior to liver in C57BL/6j mice. *Aging (Albany NY)*. 2015;7:256−268. https://doi.org/10.18632/aging.100738.
18. Hull RL, Willard JR, Struck MD, et al. High fat feeding unmasks variable insulin responses in male C57BL/6 mouse substrains. *J Endocrinol*. 2017;233:53−64. https://doi.org/10.1530/joe-16-0377.
19. Nagy C, Einwallner E. Study of in vivo glucose metabolism in high-fat diet-fed mice using oral glucose tolerance test (OGTT) and insulin tolerance test (ITT). *J Vis Exp*. 2018;131:56672. https://doi.org/10.3791/56672.
20. Winzell MS, Ahrén B. The high-fat diet-fed mouse: a model for studying mechanisms and treatment of impaired glucose tolerance and type 2 diabetes. *Diabetes*. 2004;53:215−219. https://doi.org/10.2337/diabetes.53.suppl_3.s215.
21. Jung UJ, Choi MS. Obesity and its metabolic complications: the role of adipokines and the relationship between obesity, inflammation, insulin resistance, dyslipidemia and nonalcoholic fatty liver disease. *Int J Mol Sci*. 2014;15:6184−6223. https://doi.org/10.3390/ijms15046184.
22. Joffe YT, Collins M, Goedecke JH. The relationship between dietary fatty acids and inflammatory genes on the obese phenotype and serum lipids. *Nutrients*. 2013;5:1672−1705. https://doi.org/10.3390/nu5051672.
23. Jiao P, Chen Q, Shah S, et al. Obesity-related upregulation of monocyte chemotactic factors in adipocytes: involvement of nuclear factor-kappaB and c-Jun NH2-terminal kinase pathways. *Diabetes*. 2009;58:104−115. https://doi.org/10.2337/db07-1344.
24. Lee YH, Thacker RI, Hall BE, Kong R, Granneman JG. Exploring the activated adipogenic niche: interactions of macrophages and adipocyte progenitors. *Cell Cycle*. 2014;13:184−190. https://doi.org/10.4161/cc.27647.
25. Hotamisligil GS. Inflammation and metabolic disorders. *Nature*. 2006;444:860−867. https://doi.org/10.1038/nature05485.
26. Lumeng CN, Saltiel AR. Inflammatory links between obesity and metabolic disease. *J Clin Invest*. 2011;121:2111−2117. https://doi.org/10.1172/jci57132.
27. Saltiel AR, Olefsky JM. Inflammatory mechanisms linking obesity and metabolic disease. *J Clin Invest*. 2017;127:1−4. https://doi.org/10.1172/JCI92035.

Edited by Yi Cui